Insight from the maximal activation of the signal transduction excitable network in *Dictyostelium discoideum*

Marc Edwards[a], Huaqing Cai[b], Bedri Abubaker-Sharif[a], Yu Long[a], Thomas J. Lampert[a], and Peter N. Devreotes[a,1]

[a]Department of Cell Biology, School of Medicine, Johns Hopkins University, Baltimore, MD 21205; and [b]National Laboratory of Biomacromolecules, Chinese Academy of Sciences Center for Excellence in Biomacromolecules, Institute of Biophysics, Chinese Academy of Sciences, 100101 Beijing, China

Contributed by Peter N. Devreotes, February 9, 2018 (sent for review July 6, 2017; reviewed by Richard A. Firtel and Jason M. Haugh)

Cell migration requires the coordination of an excitable signal transduction network involving Ras and PI3K pathways with cytoskeletal activity. We show that expressing activated Ras GTPase-family proteins in cells lacking PTEN or other mutations which increase cellular protrusiveness transforms cells into a persistently activated state. Leading- and trailing-edge markers were found exclusively at the cell perimeter and the cytosol, respectively, of the dramatically flattened cells. In addition, the lifetimes of dynamic actin puncta were increased where they overlapped with actin waves, suggesting a mechanism for the coupling between these two networks. All of these phenotypes could be reversed by inhibiting signal transduction. Strikingly, maintaining cells in this state of constant activation led to a form of cell death by catastrophic fragmentation. These findings provide insight into the feedback loops that control excitability of the signal transduction network, which drives migration.

signal transduction | *Dictyostelium* | cell migration | chemotaxis | waves

Cell migration is involved in a wide range of important physiological events during development and in the adult (1–3). The basic mechanisms of cell migration are well conserved across eukaryotic organisms. These processes require a coordination of signal transduction and cytoskeletal events, which regulate cellular protrusions and contractions (4). For example, in human and zebrafish neutrophils, cultured fibroblasts, and free-living amoeba, Ras GTPases and PI3K pathways control the activity of Rho GTPases which mediate the events that control the cytoskeleton (5–12). Interestingly, many of these pathways are also involved in the regulation of cell growth and metabolism, and defects in these genes transform cells (13). Often, multiple mutations are required to convert tumor cells to the most aggressive migratory phenotypes (14, 15).

Signal transduction and cytoskeletal networks display properties of excitability, leading to the propagation of waves of activation that have been observed in many cells, including neurons, neutrophils, fibroblasts, mast cells, and amoeba. In migrating *Dictyostelium* cells, coordinated waves of Ras and PI3K activation, the dissociation of PTEN, and the accumulation of phosphatidylinositol (3,4,5)-trisphosphate (PIP3) propagate along the cell cortex (5, 13–27). These waves of activity mediate the cytoskeleton-dependent protrusions and contractions, which underlie migration (28–30). These coupled networks have been designated the signal transduction excitable network (STEN) and the cytoskeleton excitable network (CEN), respectively (4, 31). Perturbations which lower the threshold for STEN activation caused the network to oscillate, which led to alternating cycles of cell spreading and contraction. However, despite the assessment of numerous single perturbations, cells were not seen to reach a persistently activated state in which negative feedback and cellular contraction were completely overwhelmed.

Such persistently activated cells would provide a powerful tool for studying the architecture of the STEN, its connection to the cytoskeletal networks, and the consequences of constant activation. First, generating a persistently and globally activated cell would overcome the experimental constraints imposed by the typically transient and localized STEN activation. Second, the response of the cytoskeletal network to an unchanging input from the STEN would better reveal the connection between the networks. Finally, in the field of oncology, there is significant interest in the pathophysiology of cells bearing activating mutations to STEN components. Typically, cells with the most aggressive migratory phenotypes still display coordinated cycles of protrusion and contraction, suggesting that the underlying signaling apparatus is not maximally activated.

There are a number of possible reasons why these experimental perturbations and oncogenic mutations failed to produce fully activated cells. Such cells could simply be unstable. Alternatively, positive feedback may be weak, or negative feedback may become overwhelming, checking further activation. Or, multiple pathways might converge on a shared output, and individual pathways cannot fully activate the network. To assess these ideas, we tested various pairwise combinations of key signal transduction and cytoskeletal network components.

Results

Morphological Consequences of Persistent STEN Activation. Since cells expressing constitutively active RasC or Rap1 or lacking

Significance

Directed cell migration is at the center of the pathophysiology of many diseases such as cancer. It requires the coordination of a signal transduction network and an underlying cytoskeleton. Understanding the composition of these networks and the mechanism by which they are coupled is critical to furthering our understanding of how cells move. Here, we have developed a cell-based tool which maximizes the activation of the signal transduction system. This has provided us with insight into its composition and the mechanism by which it controls the activity of the actin cytoskeletal activity, which drives migration. Most striking, the persistent activation of the signal transduction apparatus was discovered to have severe consequences for cell viability.

Author contributions: M.E., H.C., and P.N.D. designed research; M.E., H.C., B.A.-S., and Y.L. performed research; M.E., H.C., and T.J.L. contributed new reagents/analytic tools; M.E. and P.N.D. analyzed data; and M.E. and P.N.D. wrote the paper.

Reviewers: R.A.F., University of California, San Diego; and J.M.H., North Carolina State University.

The authors declare no conflict of interest.

[1]To whom correspondence should be addressed. Email: pnd@jhmi.edu.

This article contains supporting information online at www.pnas.org/lookup/suppl/doi:10.1073/pnas.1710480115/-/DCSupplemental.

Published online March 30, 2018.

PTEN have been reported to display flattened morphology and increased adhesion, we reasoned that combining perturbations in these pathways might have synergistic effects (Fig. 1*A*). Induction of RasC or Rap1 in wild-type AX2 cells had little effect on cell morphology. Induction of the constitutively active $RasC_{Q62L}$ or $Rap1_{G12V}$ led to moderate cell spreading, as previously reported (Fig. 1 *B*, *C*, and *E*) (13). Careful examination showed that these cells displayed morphological oscillations, rhythmically expanding and contracting in area (Fig. 1*C* and Movie S1). Cells lacking PTEN had multiple dynamic protrusions which were unaffected by the expression of RasC or Rap1 (Fig. 1 *B*, *D*, and *F*). However, induction of $RasC_{Q62L}$ or $Rap1_{G12V}$ expression in *pten*$^-$ cells led to a dramatic increase in surface area within 8 h (Fig. 1 *D* and *F* and Movie S2). In addition, the $RasC_{Q62L}$/*pten*$^-$ and $Rap1_{G12V}$/*pten*$^-$ cells no longer displayed dynamic protrusions, and their motility was essentially abolished (Movie S2). The fraction of extremely spread cells in the population increased gradually after the induction of $RasC_{Q62L}$, and tightly correlated with the expression of the protein (Fig. S1 *A* and *B*).

Further analysis showed that the volumes of the $RasC_{Q62L}$/*pten*$^-$ and $Rap1_{G12V}$/*pten*$^-$ cells were not significantly changed and that they remained mononucleated (Fig. S1*C*); however, they were extremely flat. Approximately 70% of the population adopted this morphology (Fig. S1*A*), whereas the remainder maintained the morphology of parental *pten*$^-$ cells, with no interconversions. Isosurface rendering of a field of GFP-expressing cells (Fig. 1*G*) showed that compared with parental *pten*$^-$ cells, those expressing $RasC_{Q62L}$ adopted a flattened, disk shape or "pancake" morphology (Movie S3). We defined a flatness parameter, F, as the square root of the basal surface area divided by the cube root of the volume. AX2 (wild-type) and *pten*$^-$ cells had median F values of 1.24 and 1.46, respectively (Fig. 1*H*). Upon induction of $RasC_{Q62L}$ in AX2 cells, the median flatness of the resulting population increased to 1.43. When $RasC_{Q62L}$ was induced in *pten*$^-$ cells, the resulting populations were biphasic. Thirty percent of the cells had an F value of 1.50, statistically identical to parental *pten*$^-$ cells (Fig. 1*H* and Fig. S1*A*). However, ~70% of cells had an F value >2.17 (Fig. 1*F* and Fig. S1*A*). These effects could be reversed by using the respective TorC2 and PI3K inhibitors, PP242 and LY294002, which have been previously shown to partially suppress the phenotype of *pten*$^-$ cells (Fig. 1 *I* and *J*).

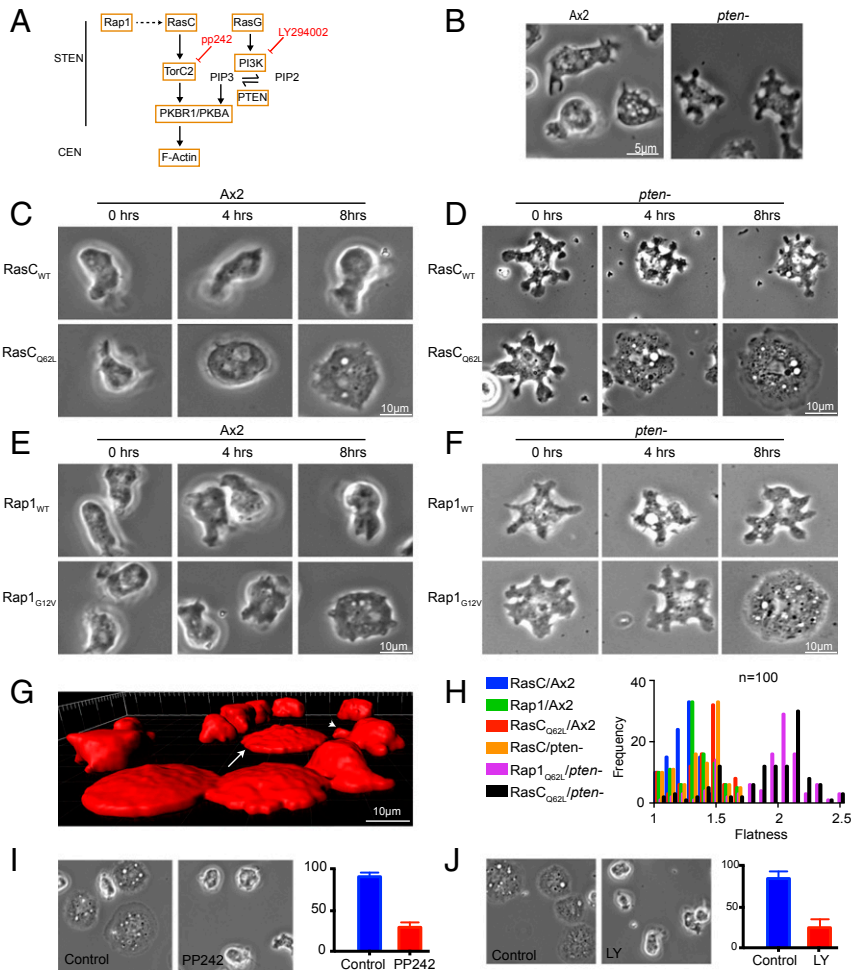

Fig. 1. $RasC_{Q62L}$ expression of constitutively active RasC or Rap1 leads to dramatic cell spreading in *pten*$^-$ cells. (*A*) Experimental scheme. Inhibitors used in this study are shown in red type. (*B*) Untransfected control cells. (*C*–*F*) Ras and Rap constructs were induced with doxycycline, and representative images were acquired at the indicated times for wild-type and constitutively active RasC expressed in (*C*) AX2 cells and (*D*) *pten*$^-$ cells, and for wild-type and constitutively active Rap1 expressed in (*E*) AX2 cells and (*F*) *pten*$^-$ cells. (*G*) Isosurface renders of RasC/*pten*$^-$ cells (arrowhead) and RsC_{Q62L}/*pten*$^-$ cells (arrow). (*H*) Distribution of flatness coefficients of AX2 and *pten*$^-$ cells expressing indicated constructs. (*I* and *J*) Inhibitions of the pancake phenotype by (*I*) PP242 and (*J*) LY294002.

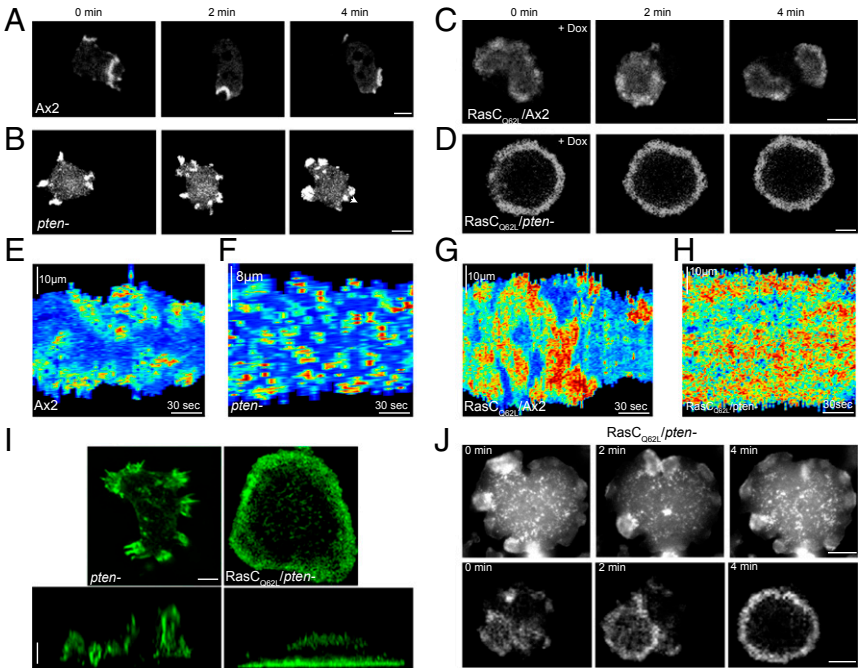

Fig. 2. Cytoskeletal changes in persistently activated cells. (*A–D*) AX2 and *pten*$^-$ cells expressing the indicated constructs and F-actin probe RFP-LimE$_{\Delta coil}$. RasC$_{Q62L}$ expression changes the dynamics of F-actin waves, producing a persistent band of peripheral staining in *pten*$^-$ cells. (Scale bars: *A–C*, 5 μm; *D*, 4 μm.) (*E–H*) Respective kymographs of cells in *A–D*. (*I*) High-resolution images of actin probe LimE in parental *pten*$^-$ (*Left*) and RasC$_{Q62L}$/*pten*$^-$ (*Right*) cells. *Top* shows a view of the ventral surface; *Bottom* shows a side profile. (Scale bars: 5 μm.) (*J*) Intermediate-wave F-actin wave pattern (GFP-LimE$_{\Delta coil}$) phenotypes induced by RasC$_{Q62L}$ expression in *pten*$^-$ cells. (Scale bars: 5 μm.) Dox, doxycycline.

Cytoskeletal Changes in Persistently Activated Cells. We next examined the actin cytoskeleton, using the F-actin biosensor LimE$_{\Delta coil}$, to determine the basis for the morphological differences between the cells. In wild-type cells, there were typically one or two LimE patches at any given moment, each occupying 10 to 15% of the perimeter and lasting for ∼90 s (Fig. 2 *A* and *E* and Fig. S2). In *pten*$^-$ cells, patches were smaller and significantly more numerous and lasted for ∼15 to 30 s (Fig. 2 *B* and *F* and Fig. S2). In RasC$_{Q62L}$-expressing cells, patches occupied a significantly larger fraction (∼40% of the cell perimeter) and often propagated laterally for 1 to 2 min during part of the oscillatory cycle (Fig. 2 *C* and *G* and Fig. S2). In RasC$_{Q62L}$/*pten*$^-$ cells, LimE appeared as a diffuse wide band around the entire perimeter, with a few fluctuations but no global oscillations (Fig. 2 *D* and *H* and Fig. S2). A lateral view of structured illumination microscopy images of these cells showed this band of LimE accumulation localized on the ventral surface, as well as an increased density of filopodialike structures on the dorsal surface of the cell (Fig. 2*I*). This morphology contrasted dramatically to parental *pten*$^-$ cells in which patches were randomly distributed about the cell surface (Fig. 2*I*).

The transition between the *pten*$^-$ and pancake phenotypes occurred via at least two intermediate paths. Observations of these transitions were rare since the transition occurred over the course of minutes in an induction process that spans hours. In some instances, the circular LimE rings near the perimeter became enlarged and more numerous (Fig. 2*J*, *Top*). Eventually, these fused into the single large peripheral ring as the cells flattened out. In other instances, a single circular wave of F-actin signal was initiated and rapidly expanded across the cell surface to generate the band at the periphery (Fig. 2*J*, *Bottom*). After the establishment of this band, additional actin waves were rarely initiated. Several experiments on fixed and live cells suggests that the diffuse band of F-actin signal at the periphery of RasC$_{Q62L}$/*pten*$^-$ cells is made up of dynamic puncta (Fig. 3 *A* and *B* and Movies S4 and S5). Previous studies have shown transient or oscillatory F-actin puncta on the basal and lateral surfaces of wild-type cells in total internal reflection fluorescence and lattice light sheet microscopy images, with lifetimes or periods of about 10 s (4, 32). In contrast, F-actin puncta within the peripheral band of the pancake cells were more long-lived, lasting for 20 to 30 s (Fig. 3*C*). The lateral spacing of these bright puncta was several times the diameter of the puncta themselves (Movie S4), suggesting that the long-lived puncta were not made up of multiple shorter events. The distribution of the durations within these three populations is shown in Fig. 3*D* and Table 1.

Evidence suggests that elevated STEN activity is responsible for the longer lifetimes of F-actin puncta. The longer-duration puncta at the perimeter of pancake cells were reverted to wild-type durations by inhibiting the PI3K and TorC2 pathways with LY294002 and PP242, respectively (Fig. 3 *E* and *F*). The inhibitors had little effect on the distribution of lifetimes of the majority of puncta in wild-type cells (Fig. 3*E*). The longer-duration puncta first revealed in pancake cells were subsequently observed in wild-type cells (Fig. S3 *A–C*). Puncta on the ventral surface of single and electrofused wild-type cells colocalized with propagating actin waves also last 20 to 40 s, whereas those outside (>2 μm from the wave boundary) of propagating waves typically last 8 to 10 s, as in wild-type cells (Fig. S3*D* and Movies S6–S8).

Localization of STEN Activity in Persistently Activated Cells. Previous studies have determined the spatial and temporal correlation of STEN and CEN activity (4, 33). We sought to determine the localization of STEN markers in the persistently activated cells. In *pten*$^-$ cells, the RasG/D biosensor RBD showed a near identical pattern to the LimE pattern described in Fig. 2, with small, 20- to 30-s patches at the cell cortex (Fig. 4 *A* and *B*). In RasC$_{Q62L}$/*pten*$^-$ cells, the RBD signal appeared as a persistent broad band at the perimeter like that seen for LimE (Fig. 4 *C*

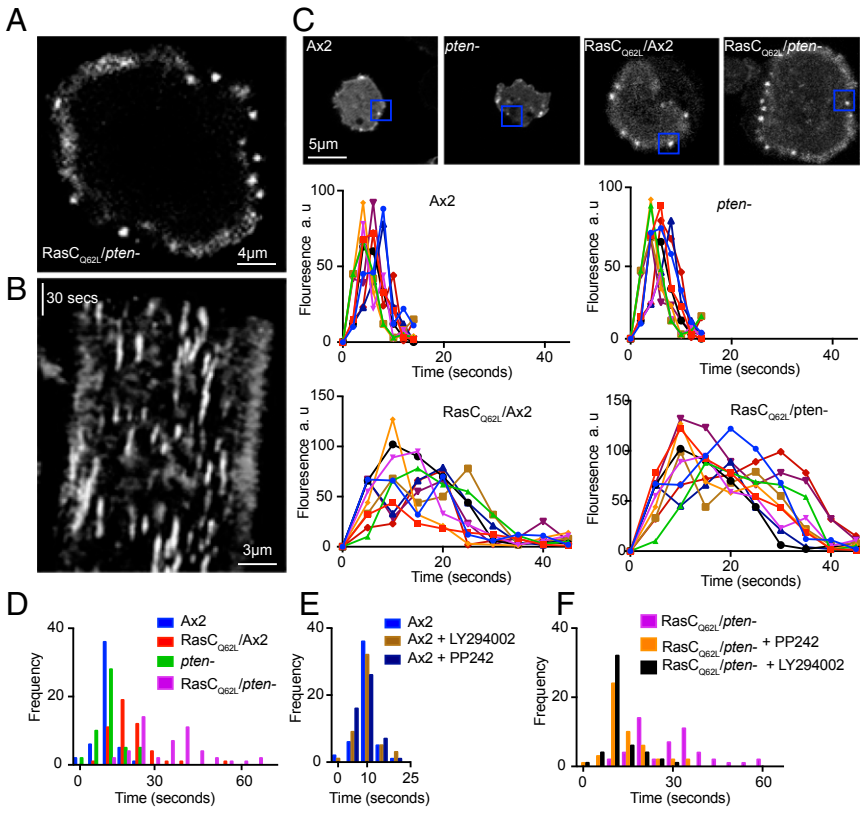

Fig. 3. Increased lifetime of F-actin puncta in persistently activated cells. (*A*) Confocal section near the ventral surface of a RasC$_{Q62L}$/*pten*$^-$ cell expressing F-actin probe-LimE$_{\Delta coil}$. (*B*) t-Stack of the cell in *A* showing lifetime of F-actin puncta. (*C*) The changes in intensity over the lifetime of 10 different F-actin puncta from cells seen in *Top* are traced in the graphs shown *Below*. Blue traces on graphs correspond to boxed puncta in *Top*. (*D–F*) Frequency distribution of puncta lifetimes. Wild-type and activated cells were treated with the indicated inhibitors for an hour before recording puncta lifetimes. Average lifetime of puncta in $n = 100$ different cells.

and *D*). Unlike the LimE pattern, however, there were no puncta in the RBD signal. To determine the extent to which our perturbations alter STEN activity, we examined the phosphorylation of PKBs and several PKB substrates. In wild-type cells, a probe (R1-Akt) for TorC2 activity was confined to the small patches at the cell periphery (Fig. 4*E*; arrows), whereas in RasC$_{Q62L}$/*pten*$^-$ cells, the signal was localized to a band at the periphery of the cell. The fraction of the cortex occupied by R1-Akt patches increased from 10 to 15% in RasC/AX2 cells to 90 to 100% in RasC$_{Q62L}$/*pten*$^-$ cells (Fig. 4*F*). To examine PKB activity in RasC$_{Q62L}$/*pten*$^-$ cells, we quantitated PKBRI phosphorylation. As expected, RasC$_{Q62L}$ expression led to a twofold increase in phosphorylation of PKBRI (Fig. 4*G* and Fig. S4). When normalized to cells expressing an empty vector, RasC$_{Q62L}$/*pten*$^-$ or Rap1$_{G12V}$/*pten*$^-$ showed an approximate threefold increase in PKB-substrate phosphorylation (Fig. 4 *H* and *I* and Fig. S4).

Together, these observations suggest that the additive effects of these pairwise perturbations can drive cells into the fully activated state. Consistently, when wild-type cells were stimulated with folic acid, LimE was recruited to the cortex, whereas there was no further enhancement of the cortical LimE signal in RasC$_{Q62L}$/*pten*$^-$ cells (Fig. S5). In addition, myosin II was largely confined to the cytosol of pancake cells, in stark contrast to its cortical localization in nonprotruding areas in both *pten*$^-$ and wild-type cells (Fig. S6; arrows). Mutants with excessive protrusions can be converted to the pancake phenotype.

To further interrogate the conditions required to generate constitutively active cells, we expressed RasC$_{Q62L}$ and Rap1$_{G12V}$ in a series of cells lines lacking different regulators of adhesion and motility (RAMs$^-$) (34) or the Hippo homolog, KrsB. We chose these mutants because they demonstrate both increased cell adhesion and multiple peripheral F-actin patches reminiscent of *pten*$^-$ cells. As shown in Fig. 5*A*, expression of RasC$_{Q62L}$ in RAMs 1$^-$, 3$^-$, 6$^-$, 8$^-$, 12$^-$, 13$^-$, and 14$^-$ and KrsB$^-$ induced the pancake cell phenotype similar to that observed when expressing RasC$_{Q62L}$ in *pten*$^-$ cells.

We focused on RAM13$^-$ cells to further characterize these phenotypes, by expressing LimE and the PIP3 biosensor PH$_{Crac}$. The multiple dynamic projections in RAM13$^-$ cells were labeled with both biosensors (Fig. 5 *B–E*). Conversion of these cells to the pancake morphology by expressing RasC$_{Q62L}$ led to the appearance of a broad persistent band of punctate LimE signal at the periphery of the cell (Fig. 5*C* and Movie S9), as was observed in the *pten*$^-$ background. Similarly, the PH$_{Crac}$ signal appeared as a persistent band at the cell periphery (Fig. 5*E*), a pattern that was shared by the STEN marker RBD in the *pten*$^-$ background (Fig. 4*D*). Together, these observations further demonstrate that the additive effects of these pairwise perturbations drive cells into a fully activated state.

Table 1. Actin puncta lifetime calculations from confocal and light sheet microscopy datasets

Cell line	Actin flash lifetime (confocal), s	Actin flash lifetime (light sheet), s
AX2	8 to 10	8 to 10
pten$^-$	8 to 12	8 to 10
AX2/RasC_Q62L	18 to 23	20 to 25
pten$^-$/RasC_Q62L	30 to 36	28 to 34

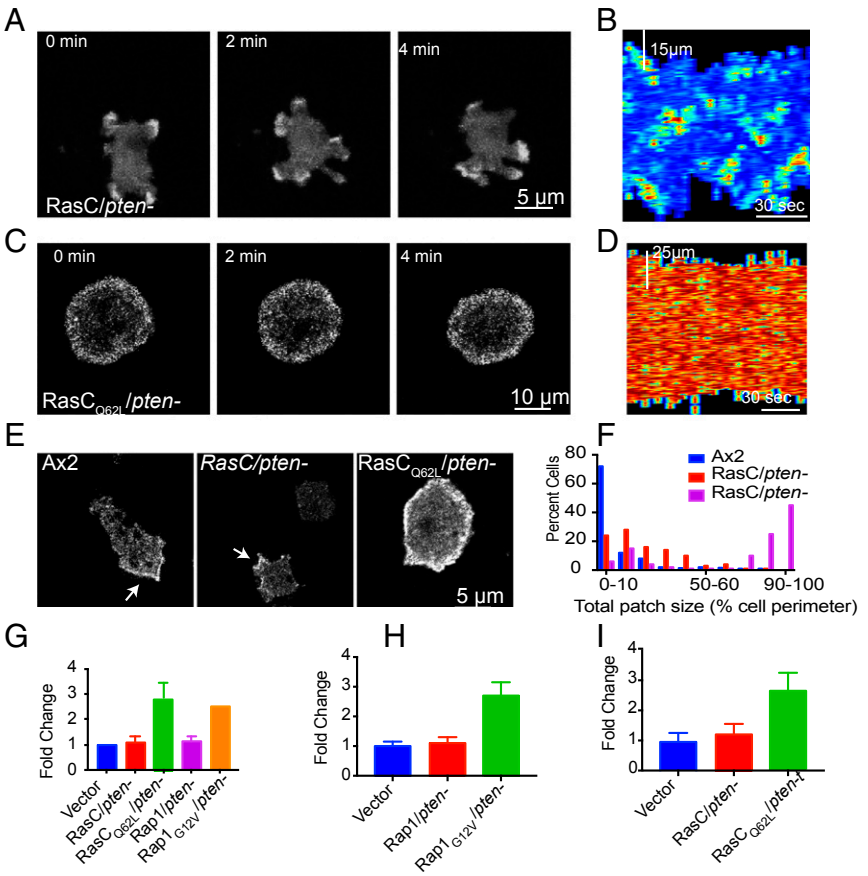

Fig. 4. Signal transduction changes in persistently activated cells. Ras-GTP probe GFP-RBD expressed in (*A*) *pten*$^-$ cells with (*B*) associated kymograph, and in (*C*) RasC$_{Q62L}$/*pten*$^-$ cells with (*D*) associated kymograph. (*E*) Representative images of cells expressing TorC2 activity probe R1-Akt; arrows indicate patches of R1-Akt signal at the cell cortex. (*F*) Portion of the cortex occupied by R1-Akt from experiments in *E*; n = 100 cells; error bars are SD. (*G–I*) P-PKBR1 levels quantified from immunoblots (*G*) show a marked increase in activated cells. PKB-substrate phosphorylation levels were similarly quantified in (*H*) Rap1$_{G12V}$- and (*I*) RasC$_{Q62L}$-activated cells. n = threefold change normalized to empty vector-transformed cells.

Physiological Consequences of Maintaining Cells in the Fully Activated State. Given the persistent band of signal transduction events and actin polymerization at the periphery of pancake cells, we reasoned that they would have difficulty with regulating actin-dependent processes. First, RasC$_{Q62L}$/*pten*$^-$ or Rap1$_{G12V}$/*pten*$^-$ cells showed a ∼10-fold reduction in their ability to engulf labeled yeast particles compared with wild-type AX2 cells (Fig. S7 *A* and *B*). Second, both *pten*$^-$ and RAM13$^-$ cells expressing RasC$_{Q62L}$ and Rap1$_{G12V}$ showed an approximate two- to threefold reduction in the rate of fluid uptake relative to wild-type AX2 cells and *pten*$^-$ controls (Fig. S7*C*). Third, RasC$_{Q62L}$/*pten*$^-$ or Rap1$_{G12V}$/*pten*$^-$ cells or other maximally activated pancake cells were more fragile and sensitive to physical manipulation than their parental counterparts (Fig. S9). We noticed an increased sensitivity of these cells to mechanical shock to the culture dish or manipulation by pipette, reminiscent of cells spread on polylysine substrate (35). We devised two tests to quantitate this increased fragility. Under shear force, 90% of the RasC$_{Q62L}$/*pten*$^-$ cells lysed at 200 rpm, whereas 75% of the parental *pten*$^-$ cells remained viable (Fig. S8*A*). Similarly, these maximally activated cells were more sensitive to hypotonic shock–induced cell death than their parental *pten*$^-$ counterparts (Fig. S8*B*).

Even in the absence of physical stress, maintaining cells in the pancake morphology for an extended period led to a striking pattern of morphological changes culminating in fragmentation. Three to 4 h after the first appearance of this flattened fully activated state (10 h after induction of RasC$_{Q62L}$ expression), the cells began to develop a deep C-shaped indentation of the perimeter at one or multiple positions (Fig. 6 *A* and *B*). This indentation was followed by a furrowing of the cell body, sometimes severing the cell into fragments (Movie S10). Alternatively, cells underwent multiple rounds of furrowing followed by a transient reversal to the original morphology, before undergoing a terminal fragmentation. The individual cellular pieces resulting from this fragmentation still displayed some limited motility but were nonviable. Replating assays performed on the population of RasC$_{Q62L}$/*pten*$^-$ or Rap1$_{G12V}$/*pten*$^-$ cells showed decreasing viability of the population over the course of the 16 h following the earliest sign of fragmentation (Fig. 6*C*). At 48 h after the induction of RasC$_{Q62L}$ or Rap1$_{G12V}$ expression in *pten*$^-$ cells, virtually no colonies formed upon replating (Fig. 6*C*). Analysis of this population of cells under the microscope revealed a field of small, immobile particles and cellular debris. KrsB$^-$ and all RAM$^-$ mutant cells expressing RasC$_{Q62L}$ showed similar loss of viability phenotype to cells expressing RasC$_{Q62L}$/*pten*$^-$ (Fig. 6*D*, Fig. S9, and Movie S11).

We explored the genetic and environmental determinants for cell death of pancake cells by fragmentation. First, expression of RasC$_{Q62L}$ in *PKBRI*$^-$/*pten*$^-$ or *PKBA*$^-$/*pten*$^-$ cells, which have second mutations that suppress the motility defects of *pten*$^-$ cells, did not generate pancake phenotypes or cause fragmentation (Fig. 7 *A–C*). In addition, both phenotypes were mitigated by expression of the dominant-negative Rap1S17N gene or the exogenous expression of GFP-Pten in RasC$_{Q62L}$/*pten*$^-$ cells (Fig.

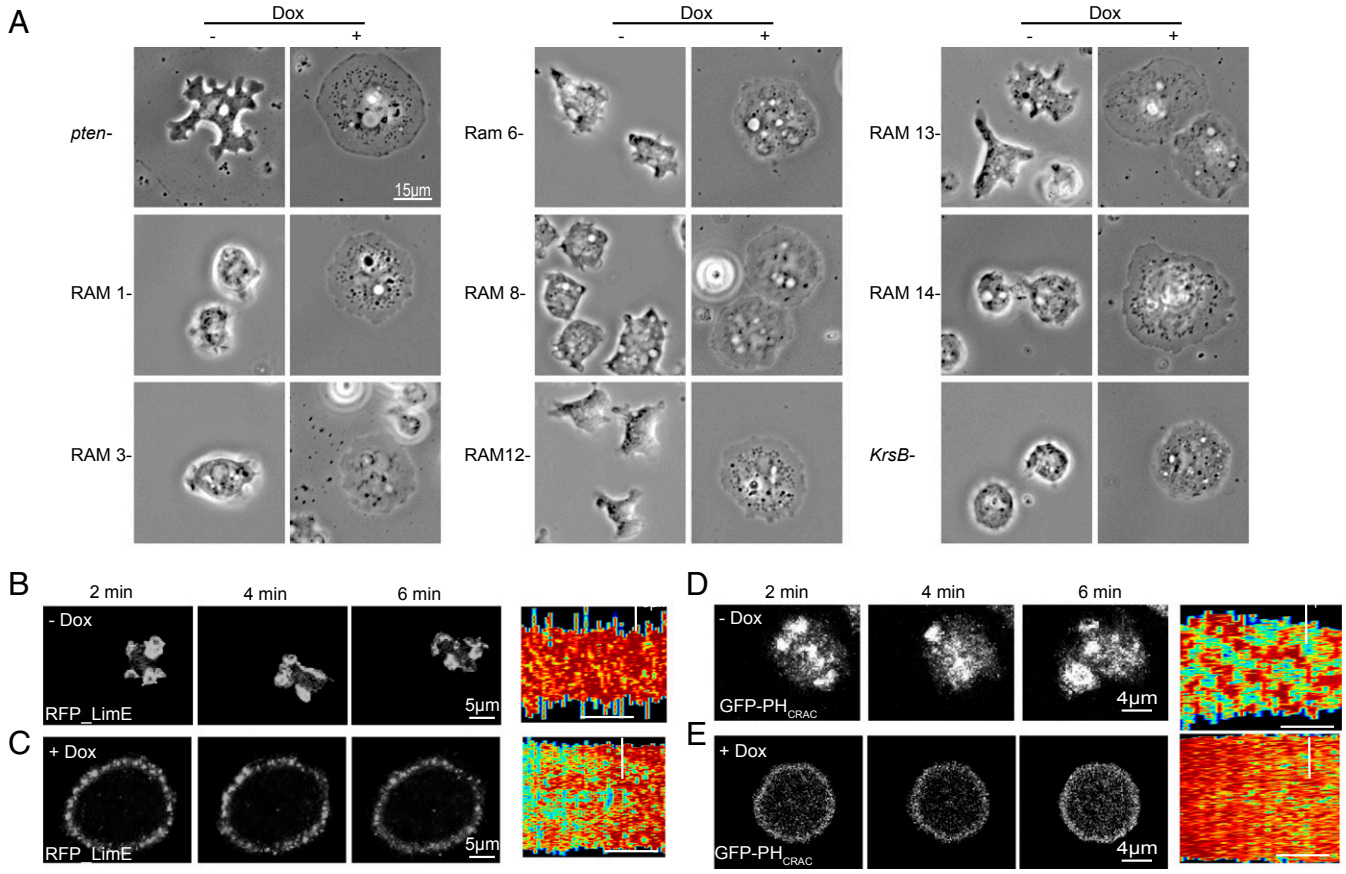

Fig. 5. Mutants with multiple protrusions can be converted to the pancake phenotype. (*A*) Expression of $RasC_{Q62L}$/$KrsB^-$ cells and RAM^- mutants induces the spread, pancake phenotype. Representative images are shown of cells before (–) and 8 h after (+) the induction of $RasC_{Q62L}$ expression by doxycycline (Dox). CON and STEN markers expressed in RAM^- pancake cells localize to a band at the periphery. (*B–E*) Selected frames from movies of $RAM13^-$ cells (*Left*) before and after induction of $RasC_{Q62L}$ with doxycycline, expressing biosensors for F-actin probe LimE (*B* and *C*) and PIP3 probe GFP-PH_{Crac} (*D* and *E*), with associated kymographs (*Right*). (Kymograph vertical scale bars: 5 μm; horizontal scale bars: 30 s.)

7*D*). In addition, as noted earlier, inhibition of TorC2 or PI3K also prevented pancake formation in $RasC_{Q62L}$/*pten*$^-$ (Fig. 7*E*). Furthermore, these manipulations were partially effective in rescuing cells already converted to the pancake morphology. Second, while $RasC_{Q62L}$/*pten*$^-$ or $Rap1_{G12V}$/*pten*$^-$ cells grew slowly in suspension, they did not fragment and remained viable for 36 h (Fig. S10*A*). However, cells induced in suspension and later plated on plastic substrate began fragmenting within 60 min, with the entire population becoming nonviable by 210 min, but when the compliance of the substrate was reduced below 16 kPa, cell death by fragmentation did not occur (Fig. S10 *B–D*).

Discussion

Our experiments demonstrate that cells can integrate multiple activating mutations, leading to a persistently activated state (Fig. 8). Many single perturbations drive wild-type cells into a partially activated phenotype best exemplified by cells lacking PTEN or expressing activated Ras producing cells with numerous or exaggerated protrusions. We have shown that combinations of these and similar activating mutations drive cells into a maximally activated state (see Table S1 for a list of perturbations). This is characterized by a permanent relocalization of leading- and trailing-edge markers to the cell perimeter and the cytosol, respectively. STEN activity drives the expansion of actin waves to the periphery of the ventral surface of the cell. This causes intense spreading and flattening and the loss of dynamic protrusive activity, motility, phagocytosis, and fluid uptake. Most striking was the increased susceptibility of these pancake- shaped cells to fragmentation, which eventually led to cell death (Fig. 8). This process is not apoptosis as described in metazoans, as *Dictyostelium* amoebae lack the requisite machinery (36, 37). We suggest the name "sparagmosis", which describes the manner in which cells tear themselves apart and die.

Models for excitable networks predict that a persistently activated state should be achieved at sufficiently low thresholds. In our previous studies, multiple different individual perturbations were able to lower the threshold for activation of the signal transduction network (18). This led to transitions in the mode of migration from amoeboid to keratocytelike and oscillatory, but not persistent, activation. Here, we have shown that our previous incapacity to generate fully activated cells was likely due to the inability of any single perturbation to completely control positive and negative feedback loops in the excitable network. The maximally activated state achieved here with multiple perturbations is characterized by the simultaneous global elevation of components involved in both positive and negative feedback loops such as Ras and PKBs, respectively (18, 38). Indeed, many of the RAM^- mutants we tested here, in addition to PTEN null cells, show elevated PKB activity (34). Together, these studies highlight the robust nature of the signaling and cytoskeletal networks involved in cell migration and more clearly define the components of the feedback loops involved in excitability.

Since their discovery by Vicker (20) over a decade ago in *Dictyostelium*, actin waves have been described in neutrophils (21) and fibroblasts (23), among other cell types. While signal transduction has been implicated in their control, a mechanism

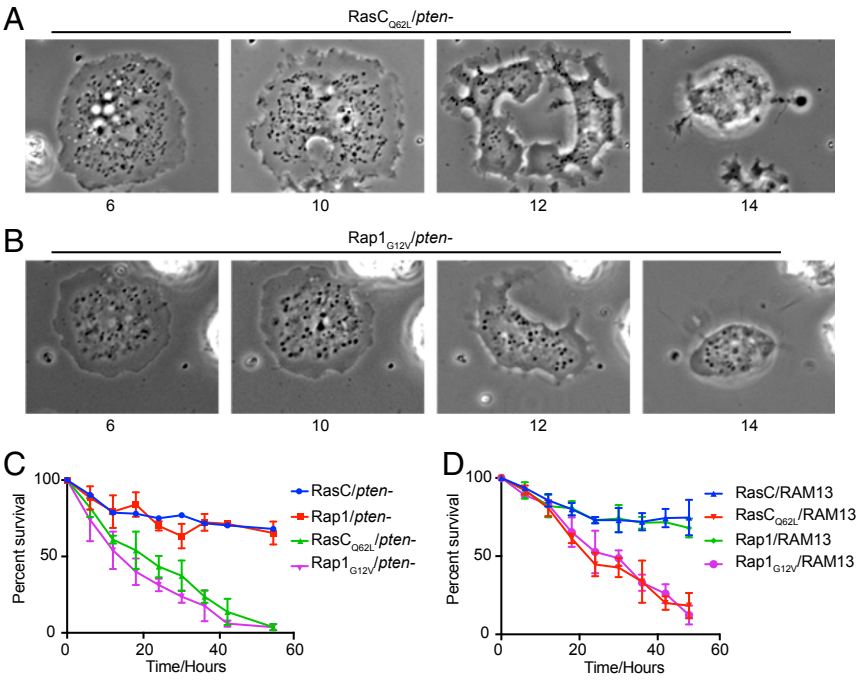

Fig. 6. Persistent activation of the STEN leads to cell death by sparagmosis. (*A*) Persistent elevation of RasC$_{Q62L}$. (Magnification: 40×.) (*B*) Rap1$_{G12V}$ signaling triggers fragmentation. (Magnification: 40×.) (*C*) Doxycline added at time 0. Sparagmosis after 8 to 10 h, leading to the precipitous decline in survival in RasC$_{Q62L}$ and Rap1$_{G12V}$ relative to control RasC and Rap1 expressing *pten*$^-$ cells. (*D*) Sparagmosis in RAM$^-$ mutants expressing RasC$_{Q62L}$ and Rap1$_{G12V}$ follows a similar time course to *pten*$^-$ cells. $n = 3$ experiments; error bars are SEM.

for this regulation has remained elusive. Observations of cytoskeletal biosensors in the pancake cells gave important insight into how the signal transduction and cytoskeletal networks are linked. Our results here show that constant STEN activity increases the overall amount of F-actin in the diffuse peripheral band, while the local puncta remain dynamic. However, the lifetime of

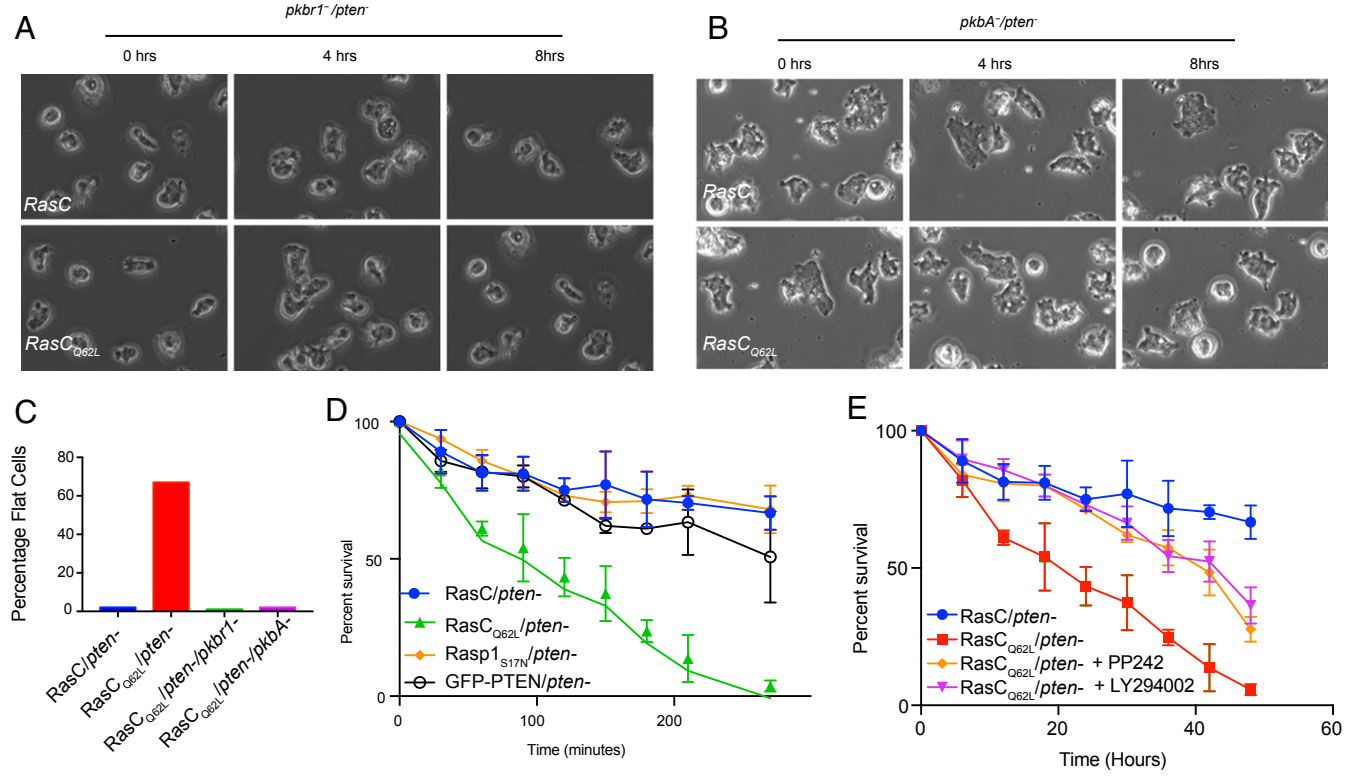

Fig. 7. The STEN is required for pancake cell formation and sparagmosis. (*A*) *pkbR1*$^-$/*pten*$^-$ and (*B*) *pkbA*$^-$/*pten*$^-$ cells are unable to form pancake cells when RasC$_{Q62L}$ expression is induced. Doxycycline was added at time 0. (*C*) Quantification of data in *A* and *B*. (*D*) Sparagmosis induction can blocked by rescuing *pten*$^-$ cells with GFP-Pten or by dominant-negative Rap1. (*E*) TorC2 inhibitor PP242 and PI3K inhibitor LY294002, when added to cells for an hour before induction of RasC$_{Q62L}$ at time 0, effectively blocked sparagmosis induction, suggesting that PKB signaling and STEN activity are required for sparagmosis. For *D* and *E*, $n = 3$ experiments; error bars are SEM.

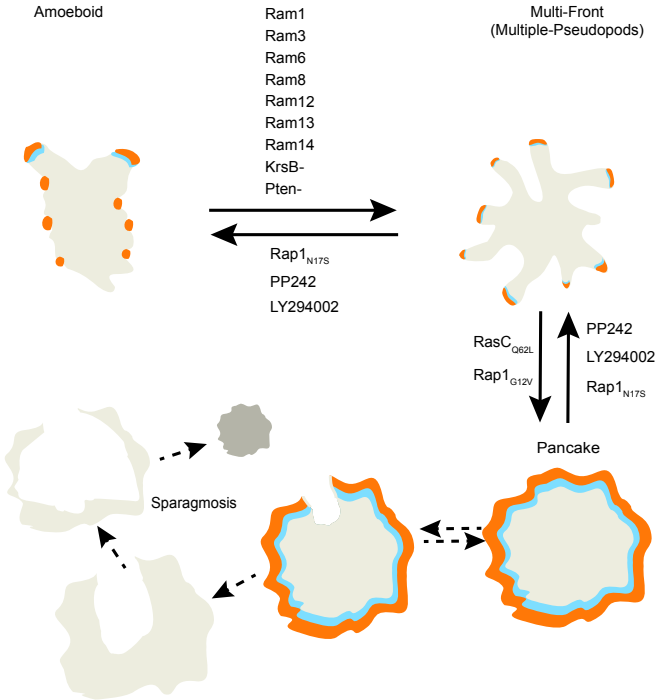

Fig. 8. Model depicting the pathways leading to maximal activation of the STEN. Pairwise combination of constitutively active RasC or Rap1 activation with mutants which increase pseudopod formation leads to maximal activation of the STEN and the induction of sparagmosis, which leads to cell death. Maximal activation requires STEN activity and can be reversed or blocked by inhibiting it.

these puncta is extended two- to fourfold. Both of these effects may contribute to the mechanism by which the propagating signal transduction waves drive out protrusions from the cell surface. Indeed, in some instances, filopodia are seen to emerge from the "rim" of expanding cuplike structures (Movie S5), possibly emanating from long-lived puncta (32). Several recent reports suggest that actin polymerization events induced mechanically with substrate perforations or ridges require simultaneous input from overlying propagating signal transduction waves (39, 40). Perhaps at higher resolution, these F-actin–rich events will be seen to be made up of puncta with enhanced duration.

Previous reports in spreading mammalian cells treated with inhibitors of nonmuscle myosin demonstrated the propensity of cells to fragment due to the loss of "cytoskeletal coherence" (41). Unfortunately, these studies were not sufficiently prolonged to determine the extent to which cells could or could not recover from this condition. In addition, at peak activation by global chemoattractant stimulation, myosin II transiently dissociates from the cortex. Consistently, the persistent activation of the signaling apparatus reported here leads to a chronic loss of cortical myosin II. We suggest that, as in mammalian cells, this leads to a loss of cytoskeletal coherence. When this is prolonged in *Dictyostelium*, death by sparagmosis ensues.

Activating mutations of the signal transduction apparatus, as occur in cancer cells, have significant effects on morphology and migration, although few studies have demonstrated as extreme an effect as we show here in *Dictyostelium*. Indeed, cancer cells in which PI3K, Ras, or Rac1 have been aberrantly activated retain the ability to extend and retract dynamic protrusions, albeit with altered morphology and dynamics (15). Activating mutations to the signal transduction apparatus lower the threshold at which protrusions are generated and, thus, increase the sensitivity of cells to motility signals. This might explain why the aberrant activation of PI3K and Ras and the inactivation of PTEN promote invasiveness in cancer cells. However, our results show that maximal activation of the signaling apparatus is ultimately deleterious to movement and, therefore, may impair invasiveness. It is generally observed that only a few driver mutations are found in any given tumor sample, despite there being a plethora of potential mutations (14, 15). Perhaps cancer cells also arrive at a point of maximal activation, and the accumulation of additional driver mutations is selected against. Common therapeutic approaches have focused on suppressing the aberrant activation of motility-promoting mutations in cancer cells, whereas our studies demonstrate that the maximal activation of the signaling apparatus may present an alternative approach.

Materials and Methods

For all experiments, *D. discoideum* AX2 strains were cultured in HL5 medium on tissue culture-treated plastic 100-mm (Greiner CELLSTAR) or 150-mm (Falcon) plates for 48 h to 80 to 90% confluency at 22 °C. Fluorescent imaging and chemotaxis assays were performed in developmental buffer (phosphate buffer supplemented with 2 mM $MgSO_4$ and 0.2 mM $CaCl_2$). Phase-contrast imaging was performed in HL5 medium. Experiments on pancake cells were performed on cells 8 to 12 h after induction, unless otherwise indicated. Complete details can be found in *SI Materials and Methods*.

1. Baumann K (2014) Stem cells: Moving out of the niche. *Nat Rev Mol Cell Biol* 15:79.
2. Weninger W, Biro M, Jain R (2014) Leukocyte migration in the interstitial space of non-lymphoid organs. *Nat Rev Immunol* 14:232–246.
3. Montell DJ (2008) Morphogenetic cell movements: Diversity from modular mechanical properties. *Science* 322:1502–1505.
4. Huang CH, Tang M, Shi C, Iglesias PA, Devreotes PN (2013) An excitable signal integrator couples to an idling cytoskeletal oscillator to drive cell migration. *Nat Cell Biol* 15:1307–1316.
5. Wang MJ, Artemenko Y, Cai WJ, Iglesias PA, Devreotes PN (2014) The directional response of chemotactic cells depends on a balance between cytoskeletal architecture and the external gradient. *Cell Reports* 9:1110–1121.
6. Swaney KF, Huang CH, Devreotes PN (2010) Eukaryotic chemotaxis: A network of signaling pathways controls motility, directional sensing, and polarity. *Annu Rev Biophys* 39:265–289.
7. Para A, et al. (2009) *Dictyostelium* Dock180-related RacGEFs regulate the actin cytoskeleton during cell motility. *Mol Biol Cell* 20:699–707.
8. Kölsch V, Charest PG, Firtel RA (2008) The regulation of cell motility and chemotaxis by phospholipid signaling. *J Cell Sci* 121:551–559.
9. Filić V, Marinović M, Faix J, Weber I (2012) A dual role for Rac1 GTPases in the regulation of cell motility. *J Cell Sci* 125:387–398.
10. Artemenko Y, Lampert TJ, Devreotes PN (2014) Moving towards a paradigm: Common mechanisms of chemotactic signaling in *Dictyostelium* and mammalian leukocytes. *Cell Mol Life Sci* 71:3711–3747.
11. Haugh JM (2002) A unified model for signal transduction reactions in cellular membranes. *Biophys J* 82:591–604.
12. Kaur H, Park CS, Lewis JM, Haugh JM (2006) Quantitative model of Ras-phosphoinositide 3-kinase signalling cross-talk based on co-operative molecular assembly. *Biochem J* 393:235–243.
13. Carracedo A, Pandolfi PP (2008) The PTEN-PI3K pathway: Of feedbacks and cross-talks. *Oncogene* 27:5527–5541.
14. Leiserson MDM, Blokh D, Sharan R, Raphael BJ (2013) Simultaneous identification of multiple driver pathways in cancer. *PLoS Comput Biol* 9:e1003054.
15. Fruman DA, Rommel C (2014) PI3K and cancer: Lessons, challenges and opportunities. *Nat Rev Drug Discov* 13:140–156.
16. Arai Y, et al. (2010) Self-organization of the phosphatidylinositol lipids signaling system for random cell migration. *Proc Natl Acad Sci USA* 107:12399–12404.
17. Asano Y, Nagasaki A, Uyeda TQ (2008) Correlated waves of actin filaments and PIP3 in Dictyostelium cells. *Cell Motil Cytoskeleton* 65:923–934.
18. Miao Y, et al. (2017) Altering the threshold of an excitable signal transduction network changes cell migratory modes. *Nat Cell Biol* 19:329–340.
19. Taniguchi D, et al. (2013) Phase geometries of two-dimensional excitable waves govern self-organized morphodynamics of amoeboid cells. *Proc Natl Acad Sci USA* 110:5016–5021.
20. Vicker MG (2002) Eukaryotic cell locomotion depends on the propagation of self-organized reaction-diffusion waves and oscillations of actin filament assembly. *Exp Cell Res* 275:54–66.
21. Weiner OD, Marganski WA, Wu LF, Altschuler SJ, Kirschner MW (2007) An actin-based wave generator organizes cell motility. *PLoS Biol* 5:e221.
22. Xiao Z, Zhang N, Murphy DB, Devreotes PN (1997) Dynamic distribution of chemoattractant receptors in living cells during chemotaxis and persistent stimulation. *J Cell Biol* 139:365–374.

23. Case LB, Waterman CM (2011) Adhesive F-actin waves: A novel integrin-mediated adhesion complex coupled to ventral actin polymerization. *PLoS One* 6:e26631.
24. Nishikawa M, Hörning M, Ueda M, Shibata T (2014) Excitable signal transduction induces both spontaneous and directional cell asymmetries in the phosphatidylinositol lipid signaling system for eukaryotic chemotaxis. *Biophys J* 106:723–734.
25. Gerisch G, Ecke M (2016) Wave patterns in cell membrane and actin cortex uncoupled from chemotactic signals. *Methods Mol Biol* 1407:79–96.
26. Gerisch G, Ecke M, Wischnewski D, Schroth-Diez B (2011) Different modes of state transitions determine pattern in the phosphatidylinositide-actin system. *BMC Cell Biol* 12:42.
27. Giannone G, et al. (2007) Lamellipodial actin mechanically links myosin activity with adhesion-site formation. *Cell* 128:561–575.
28. Tang Y, Othmer HG (1995) Excitation, oscillations and wave propagation in a G-protein-based model of signal transduction in *Dictyostelium discoideum*. *Philos Trans R Soc Lond B Biol Sci* 349:179–195.
29. Hoeller O, et al. (2016) Gβ regulates coupling between actin oscillators for cell polarity and directional migration. *PLoS Biol* 14:e1002381.
30. Devreotes P, Horwitz AR (2015) Signaling networks that regulate cell migration. *Cold Spring Harb Perspect Biol* 7:a005959.
31. Devreotes PN, et al. (2017) Excitable signal transduction networks in directed cell migration. *Annu Rev Cell Dev Biol* 33:103–125.
32. Chen BC, et al. (2014) Lattice light-sheet microscopy: Imaging molecules to embryos at high spatiotemporal resolution. *Science* 346:1257998.
33. Bear JE, Haugh JM (2014) Directed migration of mesenchymal cells: Where signaling and the cytoskeleton meet. *Curr Opin Cell Biol* 30:74–82.
34. Lampert TJ, et al. (2017) Shear force-based genetic screen reveals negative regulators of cell adhesion and protrusive activity. *Proc Natl Acad Sci USA* 114:E7727–E7736.
35. Clarke M, Schatten G, Mazia D, Spudich JA (1975) Visualization of actin fibers associated with the cell membrane in amoebae of *Dictyostelium discoideum*. *Proc Natl Acad Sci USA* 72:1758–1762.
36. Olie RA, et al. (1998) Apparent caspase independence of programmed cell death in *Dictyostelium*. *Curr Biol* 8:955–958.
37. Tresse E, Giusti C, Kosta A, Luciani MF, Golstein P (2008) Autophagy and autophagic cell death in *Dictyostelium*. *Methods Enzymol* 451:343–358.
38. Charest PG, et al. (2010) A Ras signaling complex controls the RasC-TORC2 pathway and directed cell migration. *Dev Cell* 18:737–749.
39. Driscoll MK, Sun X, Guven C, Fourkas JT, Losert W (2014) Cellular contact guidance through dynamic sensing of nanotopography. *ACS Nano* 8:3546–3555.
40. Jasnin M, Ecke M, Baumeister W, Gerisch G (2016) Actin organization in cells responding to a perforated surface, revealed by live imaging and cryo-electron tomography. *Structure* 24:1031–1043.
41. Cai Y, et al. (2010) Cytoskeletal coherence requires myosin-IIA contractility. *J Cell Sci* 123:413–423.